Available online at www.sciencedirect.com

ScienceDirect

Advances in Space Research 56 (2015) 1806–1814

ADVANCES IN SPACE RESEARCH (a COSPAR publication)

www.elsevier.com/locate/asr

Effect of updated relaxation rate constants on the H_2O vibrational level populations and ro-vibrational spectra in the mesosphere and lower thermosphere

R.O. Manuilova [a,*], A.G. Feofilov [b], A.A. Kutepov [c], V.A. Yankovsky [a]

[a] Faculty of Physics, St. Petersburg State University, Ulianovskaya Street, 3, Petrodvorets, St. Petersburg 198504, Russia
[b] Dynamic Meteorology Laboratory, LMD/École Polytechnique, 91128 Palaiseau Cedex, France
[c] Department of Physics, The Catholic University of America, 620, Michigan Ave, NE Washington DC 20064, USA

Received 30 September 2014; received in revised form 28 November 2014; accepted 1 December 2014
Available online 16 December 2014

Abstract

This paper discusses the formation mechanisms of infrared radiation in H_2O ro-vibrational bands in the mesosphere and lower thermosphere (MLT). At these heights and above, the vibrational levels of the molecules involved in radiative transitions are not in local thermodynamic equilibrium (LTE) with the surrounding medium, and the biggest uncertainty source in modeling the IR radiation in molecular bands is associated with the corresponding vibrational kinetics model parameters. In this study, we re-analyze available experimental data of Barnes et al. (2004) and Zittel and Masturzo (1991) and update the rate constant of V–V exchange (k) corresponding to the second vibrational number v_2 increase by two and the first (or the third) quantum number decrease by one. The estimated values of k for quenching by N_2 and O_2 are 1.7×10^{-12} and 1.3×10^{-12} cm^3 s^{-1}, respectively. These values are about four times larger than the values used in all earlier models of non-LTE populations of vibrational levels and IR radiation in ro-vibrational bands of H_2O. We state that using the same k for all processes of vibrational–vibrational energy exchange does not correspond to laboratory experiments and can lead to offsets both in calculating the vibrational level populations and in H_2O concentration retrievals from IR spectral radiance. We provide the estimates of these offsets as well as a list of spectral microwindows, in which H_2O radiance is sensitive to uncertainty of k.

Keywords: H_2O vibrational relaxation; Non-LTE infrared atmospheric spectral radiance; Water vapor concentration retrievals

1. Introduction

In the middle atmosphere of Earth, water vapor plays one of the key roles by influencing the composition and energy budget of this region: the absorption of solar shortwave radiation in H_2O bands gives rise to chemically active constituents, such as OH, $O(^1D)$, H_2, and H, and their subsequent recombination results in atmospheric heating. Radiative cooling occurs mainly in the H_2O rotational band and its magnitude is small compared to that of CO_2 and O_3 vibrational bands, but the water vapor controls the concentration of ozone in the mesosphere and lower thermosphere (MLT), affecting the energetics of this part of the atmosphere. Water vapor is also a necessary component for the formation of polar mesospheric ice clouds (PMCs), a phenomenon associated with extremely low temperatures in the summer mesopause, which is believed to be an early warning system for climate changes.

Understanding the mechanisms of the H_2O radiance formation in ro-vibrational bands is important (a) to interpret the observations of the infrared (IR) atmospheric emissions of the Earth and (b) to estimate the energetic effects associated with water vapor. Due to rapid development of

* Corresponding author. Tel.: +7 8124289955; fax: +7 8124287240.
E-mail address: nansey@yandex.ru (R.O. Manuilova).

http://dx.doi.org/10.1016/j.asr.2014.12.002
0273-1177/

advanced instrumentation, long-term series of the H_2O radiance in the 1.4–6.3 μm become available. The main method of H_2O concentration retrieval in the MLT is the inversion of 6.3 μm band radiance measured in limb geometry. The interpretation of this radiance is linked with the estimation of the $H_2O(\nu_2)$ level populations, which are not in local thermodynamic equilibrium (LTE) with the surrounding medium above ~50 km altitude where the frequency of inelastic molecular collisions is not sufficient to dominate other population/depopulation mechanisms of the molecular vibrational levels (see Section 2 for more details). The populations of higher vibrational levels, the transitions from which form 1.4, 1.9, 2.7, 3.2, and 4.7 μm bands are not in LTE even at lower heights.

Modeling the IR radiation in ro-vibrational H_2O bands at the altitudes where the LTE assumption is not valid (non-LTE modeling) is a complicated task since the vibrational level populations at any given height depend on the radiation coming from the other atmospheric layers while the radiative transfer depends on the distribution of vibrational level populations in the atmospheric column, so the problem becomes non-local and non-linear. The methods of solving the problems of this kind for planetary upper atmospheres have been developed and tested on a number of applications, and it has been shown that the biggest uncertainty source is associated with that of the vibrational kinetics model parameters for the molecule under consideration (Feofilov et al., 2009, 2012; Funke et al., 2012). For H_2O, these are the processes of intramolecular vibrational–vibrational (V–V) energy exchanges occurring at the collisions with atmospheric molecules and atoms. Currently, the experimental data for these processes are available only for the transitions involving the lowest vibrational levels. The higher the energy of the vibrational level, the more speculative assumptions are used for estimating the rate constants of collisional transitions from these levels.

In this study, we describe the current status of the H_2O non-LTE models and the mechanisms of the IR radiation formation in H_2O bands (Section 2), update the value of one of the V–V rate constants based on the analysis of currently available experimental data (Barnes et al., 2004), and estimate the effect of the updated rate constant on the H_2O vibrational level populations and simulated atmospheric radiation (Section 3). In Section 4, we discuss the uncertainties of the H_2O concentration retrieval associated with this rate constant. Section 5 concludes the work.

2. Non-LTE model of H_2O molecule

2.1. The basics of non-LTE

If the frequency of inelastic molecular collisions is high, the populations of molecular vibrational levels are in local thermodynamic equilibrium with thermal reservoir and they follow the Boltzmann distribution with the local kinetic temperature T_{kin}. However, for each vibrational level in planetary atmospheres there is a height (or pressure) where other processes start influencing its population, so one has to consider them in the model. In general, the set of processes consists of: (a) the direct absorption of solar radiance; (b) absorption of the IR radiance coming from the warmer and denser lower atmosphere; (c) vibrational–translational (V–T) energy exchanges by collisions with molecules and atoms of other atmospheric constituents; (d) collisional vibrational–vibrational (V–V) energy exchange with other molecules; (e) chemical and photochemical excitation. Some of them, namely, (a), (b), and (e) are non-local in a sense that the excitation source or sink is external for a given atmospheric volume. In addition, a local process (d) can transfer excitation from the level pumped by non-local processes. If the non-local processes become noticeable w.r.t. the local ones, the LTE assumption is no longer valid, and the populations must be found at each height by solving the self-consistent system of kinetic equations and a radiative transfer equation expressing the balance relations between processes (a)–(d). The resulting vibrational level populations can be conveniently represented in the form of vibrational temperatures that give an insight into the pumping and quenching mechanisms for a given level. The vibrational temperatures T_{vib} describe the excitation degree of the level l against the ground level 0:

$$\frac{n_l}{n_0} = \frac{g_l}{g_0} \cdot e^{-(E_l - E_0)/kT_{vib}} \quad (1)$$

where n_l, g_l, E_l and n_0, g_0, E_0 are populations, statistical weights, and energies of the level l and the ground level, respectively. If $T_{vib} = T_{kin}$ the level is in LTE. If $T_{vib} > T_{kin}$ then the net pumping of the level is larger than that under LTE conditions. Similarly, if $T_{vib} < T_{kin}$, the level is populated less efficiently and/or depopulated faster than at LTE.

2.2. The non-LTE model of H_2O

In general, the non-LTE model of an arbitrary molecule consists of a set of vibrational levels, each with a subset of rotational levels, a set of optical transitions, a set of collisional rate constants for processes (c) and (d) in Section 2.1, and a set of chemical and photochemical reactions (e). For practical applications, there is a tradeoff between the number of levels involved in the non-LTE problem and the speed of the calculations. One has to keep in mind that adding more levels does not necessarily improve the accuracy of the model since not all of them are involved in energy exchange processes. A rule of thumb is to include solar-pumped levels and the levels below, which directly participate in energy redistribution.

As for the non-LTE model of H_2O, its complexity changed from 5-level one (Manuilova and Shved, 1985) through a 7-level model of López-Puertas et al. (1995), a 14-level model of (Manuilova et al., 2001; Feofilov et al., 2009), and to a 25-level model of (Funke et al., 2012), which

utilizes 21 levels of the main isotope molecule up to 050, 031, 130, 210 and 012 at 9000 cm^{-1}; two lower levels of isotope $H_2^{18}O$ and two lower levels of isotope $H_2^{17}O$. For our purposes, it is sufficient to use a 14-level model described in (Feofilov et al., 2009), where it was coupled with the kinetics model of O_2/O_3 photodissociation products (for the latest updates, see also (Yankovsky and Babaev, 2011)). The diagram in Fig. 1 shows the ground and 13 excited vibrational levels of H_2O molecule up to 7445 cm^{-1}. The levels are marked in accordance with the (v_1, v_2, v_3) vibrational quanta number where v_1 stands for symmetric stretch vibrations, v_2 refers to covalent bond bending mode, and v_3 denotes asymmetric stretch mode. Below, we provide only the details of the vibrational kinetic scheme important for the present study. The main processes of vibrational energy exchange in atmospheric H_2O are the following:

$$H_2O(v_1, v_2, v_3) + O2(0) \leftrightarrow H_2O(v_1, v_2 - 1, v_3) + O_2(1) \quad (2)$$

$$H_2O(v_1, v_2, v_3) + M \leftrightarrow H_2O(v_1 + 1, v_2, v_3 - 1) + M) \quad (3)$$

$$H_2O(v_1, v_2, v_3) + M \leftrightarrow H_2O(v_1 - 1, v_2, v_3 + 1) + M \quad (4)$$

$$H_2O(v_1, v_2, v_3) + M \leftrightarrow H_2O(v_1, v_2 - 1, v_3) + M \quad (5)$$

$$H_2O(v_1, v_2, v_3) + M \leftrightarrow H_2O(v_1 - 1, v_2 + 2, v_3) + M \quad (6)$$

$$H_2O(v_1, v_2, v_3) + M \leftrightarrow H_2O(v_1, v_2 + 2, v_3 - 1) + M \quad (7)$$

where M is N_2, O_2 or O. Process (2) describes fast quasi-resonant transition between the v_2-excited vibrational levels of H_2O and $O_2(v = 1)$ levels. Among these processes, the most important ***inter-molecular*** V–V energy exchange is the one between the first excited vibrational levels of H_2O (010) and $O_2(v = 1)$. Processes (3) and (4) are the fastest ones among the ***intra-molecular*** V–V exchanges for (200, 101, 002); (120, 021); (110, 011) and (100, 001), which are close in energy. Processes of type (5) are ***intra-molecular*** V–V transitions (040–030), (030–020), (020–010), and V–T transition (010–000), at which the second vibrational number v_2 decreases by one and the first and third quantum numbers remain the same. Processes (6) and (7) are ***intra-molecular*** V–V exchanges corresponding to the second vibrational number v_2 increase by two and the first or the third quantum number decrease by one. In our set of vibrational levels, the vibrational quanta number change in (6) and (7) can be written as: (200–120), (101–021), (101–120), (002–021); (120–040), (021–040); (110–030), (011–030) and (001–020), (100–020).

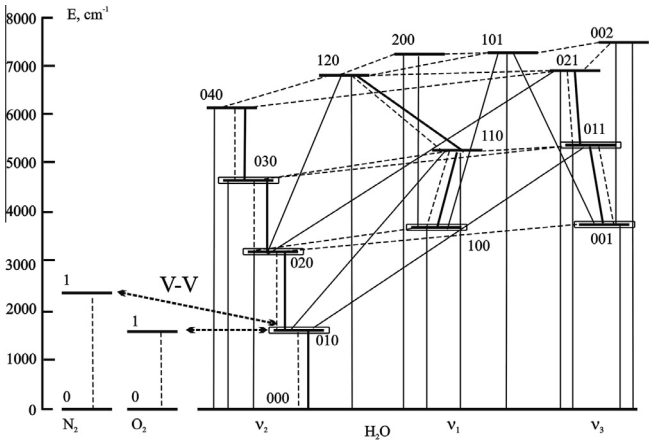

Fig. 1. Vibrational level and main processes involved into the H_2O non-LTE model. Solid lines: optical transitions; dashed lines: V–V and V–T energy exchange processes.

2.3. Rate constant for V–V energy exchange of type (6) and (7)

In this work, we focus on the processes (6) and (7). The rate constants for these processes are known only for the lowermost vibrationally excited states, namely, for transitions (001, 100) → 020 (Finzi et al., 1977). In all previous models of vibrational kinetics of H_2O molecule (Manuilova and Shved, 1985; López-Puertas et al., 1995; Funke et al., 2012) as well as in our model (Manuilova et al., 2001; Feofilov et al., 2009) it was supposed that rate constants of all processes of type (6) and (7) are equal to the rate constants for the lowermost vibrationally excited states 001, 100 measured by Finzi et al. (1977). However, proper attention was not paid to the work of Barnes et al. (2004) who studied the collisional relaxation of H_2O molecules from the highly excited (004) and (400) vibrational states in collisions with H_2O, Ar, H_2, N_2, and O_2 at transitions 004 → 023 and 400 → 320 at 293 K. In this experiment, the $H_2O(004)$ state was populated by direct absorption of dye laser radiance tuned to 719 nm. The splitting between (004) and (400) vibrational states is just 2.6 cm^{-1} and fast reaction (3) leads to efficient redistribution of pumping, so they can be considered as a quasi "super-level". The population of this level was observed with the help of a frequency-quadrupled Nd: YAG laser, which selectively photo-dissociated H_2O (400, 004), and a frequency-doubled dye laser, which observed the produced $OH(v = 0)$ via laser-induced fluorescence. The delay between the pulses of the pumping, of the photolysis, and of the probe lasers was varied to study the decay processes. The rate constants for relaxation of H_2O (400, 004), obtained from these experiments, are:

$$k(N_2) = (7.7 \pm 1.5) \times 10^{-12} cm^3\ s^{-1} \text{ and } k(O_2) = (6.7 \pm 1.4) \times 10^{-12}\ cm^3\ s^{-1} \quad (8)$$

To rescale the rate constants for processes of type (6) and (7) for the lower energy levels, Barnes et al. (2004) supposed that the values of rate constants for relaxation by Ar and H_2O depend on the vibrational quantum number n, which is equal to 4 for 004 or 400, 3 for 003, 300, and so on, and on the energy discrepancy ΔE for processes (6) and (7). Barnes et al. (2004) supposed that $ln\ (k_n/n)$ is directly proportional to $\Delta E/hc$ and estimated the rate constants for processes of type (6) and (7) for low energy levels

by interpolating between their results and the experimental data of Finzi et al. (1977) for transitions H_2O (001, 100) → 020 in collisions with Ar and H_2O.

The experiment of Barnes et al. (2004) was the first study where the rate constants of relaxation of the high energy vibrational levels were measured for collisions with N_2 and O_2. However, the first experimental data on relaxation rate constants for vibrational levels with energies higher than that of 001 and 100 were presented by Zittel and Masturzo (1991), who measured them for the H_2O(011, 110) → 030 self-relaxation and collisions with Ar. For the latter, Zittel and Masturzo (1991) estimated the upper limit of the rate constant of this transition to be equal to $(6.0 \pm 0.2) \times 10^{-13}$ cm^3 s^{-1}. In accordance with measurements of Finzi et al. (1977) the rate constant of the (001, 100) → 020 transition at collisions with Ar is $(1.4 \pm 0.2) \times 10^{-13}$ cm^3 s^{-1}. This means that the ratio of the rate constant of the (011, 110) → 030 transition to that of the (001, 100) → 020 transition is more than 4. The results of Barnes et al. (2004) and Zittel and Masturzo (1991) led us to the conclusion that the rate of energy transfer from the symmetric and asymmetric stretch modes ν_1 and ν_3 to the bending mode ν_2 (processes 6 and 7) increases with vibrational level energy.

Using the extrapolation method of Barnes et al. (2004), we have estimated k, the rate constant of transitions (002, 101) → 021 and (101, 200) → 120 to be $k(Ar) = 6.9 \times 10^{-13}$ cm^3 s^{-1}, $k(N_2) = 1.7 \times 10^{-12}$ cm^3 s^{-1}, $k(O_2) = 1.3 \times 10^{-12}$ cm^3 s^{-1} for quenching by Ar, N_2, and O_2, respectively. As one can see, using this approach leads to the same estimates of the rate constant for quenching by Ar as in Table IV in Barnes et al. (2004). However, the estimates for quenching by N_2 and O_2 are about four times larger than that measured by Finzi et al. (1977) for (001, 100) → 020 transitions. We have to note here that the discrepancy between laboratory measurements, theoretical estimates, and atmospheric retrievals of the same rate coefficient is not new in atmospheric sciences: the most important problem for the MLT is a quenching rate of $CO_2(\nu_2)$ levels for the collisions with atomic oxygen (Feofilov et al., 2012 and references therein).

To estimate the maximal effect of the updated rate constant k, we assumed that the rate constants for all processes of type (6) and (7), except for the (001, 100) → 020 transition, are equal to k. For the latter, the measurements of Finzi et al. (1977) were taken. The populations of vibrational levels and spectra of limb radiation in ro-vibrational H_2O bands were calculated for typical atmospheric scenarios and compared with those obtained for a "standard" set of rate constants used in Feofilov et al. (2009).

3. Sensitivity of vibrational level populations to rate constant *k*

3.1. Numerical experiment

The details of non-LTE calculations for the H_2O vibrational level populations are described in Section 3.2 of Feofilov et al. (2009). For this study, the calculations were carried out with the help of the non-LTE research code ALI-ARMS developed by Kutepov et al. (1998), Gusev and Kutepov (2003), and Feofilov and Kutepov (2012). As in the latter work, we have taken 5 typical atmospheric scenarios (see their Table 1 and Figs. 5 and 6), from subarctic summer to subarctic winter. Pressure/temperature profiles, O_2, and N_2 volume mixing ratio (VMR) profiles were obtained from the MSIS-E-90 database (http://omniweb.gsfc.nasa.gov/vitmo/msis_vitmo.html). Vertical distributions of atomic oxygen VMR were obtained from the SABER (Russell et al., 1999) V2.0 (http://saber.gatcInc.com/) July averages for given locations and SZA values. The vertical distribution of H_2O VMR was built using July averages retrieved from all ACE-FTS measurements (see Bernath et al. (2005)). The results are shown only for the subarctic summer model, SAS, since its kinetic temperature profile is characterized by a large (~75 K) temperature difference between the stratopause and the mesopause, revealing more non-local effects in vibrational level populations than for the other atmospheric models (radiative transfer from warmer stratopause leads to a stronger pumping of vibrational states in the cold mesosphere). The results obtained for other atmospheric models are similar to that of SAS, but the magnitude of the effects are somewhat smaller. Solar zenith angle of 46.5° corresponds to local noon conditions at 70 N for the summer solstice in the northern hemisphere.

3.2. H_2O vibrational level populations

We have obtained the non-LTE $H_2O(\nu_1, \nu_2, \nu_3)$ populations for all levels of the model at all altitudes from 0 to 150 km for two sets of rate constants: a "standard" one and an "updated" one. For the sake of clarity, in Fig. 2a the populations for an updated set are shown in the 40–110 km interval. The populations are presented in the form of vibrational temperatures (see Eq. (1)). As one can see, the 010 level is in LTE below 70 km height. The population of this level is more affected by absorption of atmospheric radiation than by absorption of solar radiation in the 6.3 μm fundamental band and other bands. Pumping from below moves the 010 out of LTE in the mesosphere, but this effect is small compared to the LTE breakdown for the uppermost levels in Fig. 1, which is due to direct absorption of solar radiance in all bands, from 1.4 to 6.3 μm. The lower vibrational states are also pumped by energy transferred from higher levels through chains of V−V and V−T exchanges. As Fig. 2a shows, at the altitude of 80–85 km, the vibrational temperatures of 020, 030, 040, and 200 levels reach the values of 350, 430, 500, and 650 K, respectively. We draw reader's attention to the fact that vibrational temperatures are used for convenience of representation, but the ratio of simulated populations w.r.t. LTE conditions is many orders of magnitude (for example, substituting $T_{vib}(020)$ from Fig. 2a to Eq. (1) gives ~7e7 w.r.t. to the LTE population). Fig. 2b represents the "updated vs standard" differences in vibrational tempera-

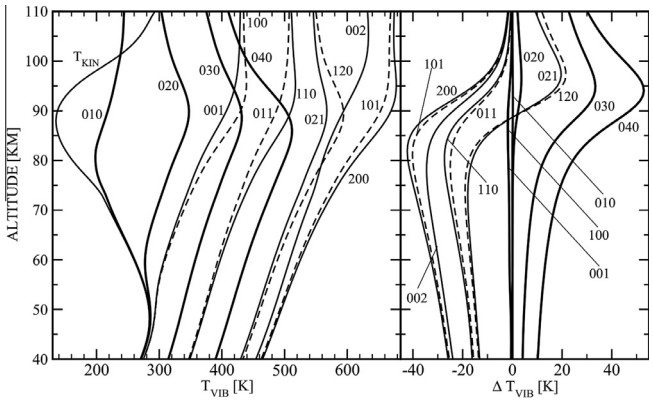

Fig. 2. Sensitivity of vibrational level populations to changes in k. (a) Vibrational temperatures for an "updated" set of rates; (b) "updated vs standard" differences in vibrational temperatures. Both solid and dashed lines in (a) and (b) are used for vibrational temperatures and their differences, respectively. Different line styles are used for the sake of visibility.

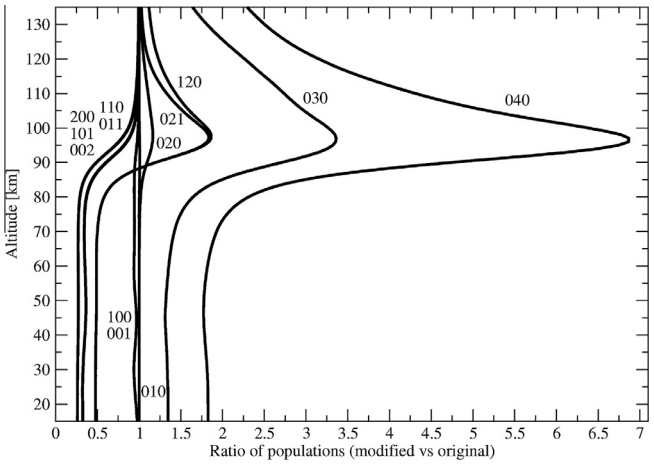

Fig. 3. Ratio of populations calculated with an updated set of rates to populations calculated for standard ones. The figure complements Fig. 2b.

tures. As one can see, the effects of k variation are negligible for 100, 010, and 001 levels while some higher vibrational states demonstrate high sensitivity to k.

It is interesting to note that above 80–85 km the T_{vib} calculated for an "updated" rate constants exceed that for "standard" ones for levels with bending mode quantum number 2, 3 and 4. For 040, this excess reaches 45 K at 95 km. Meanwhile, for the other levels and even for levels 021, 120 below 85 km the T_{vib} calculated with updated rate constants are smaller than the ones calculated for "standard" rate constants. For level 200, this difference reaches 40 K at 85 km (this corresponds to ~3 time difference in level's population, see Fig. 3, which complements Fig. 2b). The behavior of T_{vib} differences in Fig. 2b and population ratio in Fig. 3 is explained by kinetic mechanisms for the corresponding levels: stronger quenching of the upper 3 levels in our model leads to decrease of their populations, transferring more energy from these levels to lower-lying 040 and 030, which demonstrate an increase in population in the middle atmosphere. The 110 and 011 levels also act as donors to lower-lying levels while 021 and 120 work as donors below ~90 km height and as acceptors above this height. One has to note, however, that the discussion of vibrational level population above 90 km does not have much practical sense since the H_2O VMR decreases rapidly with height, and, in general, is less than 1 ppmv in this area. It is important to note that the ratio of the 010 populations is close to a unit at all heights.

4. Sensitivity of the integrated and spectral limb radiance to rate constant *k*

In addition to calculating the vibrational level populations, we have simulated limb radiation as if satellite instruments had registered it with high and low spectral resolution. The non-LTE populations calculated by ALI-ARMS were used for monochromatic limb radiance calculations for each limb-path which then were convolved either with a narrow triangular or with a broadband rectangular instrumental function to simulate observations by spectrometer or radiometer, respectively. For limb calculations, we utilized a radiative transfer module of the ALI-ARMS code validated against other limb calculations in Feofilov et al. (2009). The total number of H_2O spectral lines involved in limb calculation is ~17,000 with spectral information coming from the HITRAN database (Rothman et al., 2009). The calculations have been performed for a set of vibrational level populations obtained with a standard k and for the same set obtained with an updated k. The results are compared in Figs. 4–6. As expected, the peculiarities of the vibrational level populations can be traced in the integrated limb radiances for the H_2O ro-vibrational bands. Fig. 4 shows that the ratio of integrated limb intensities calculated for an updated set of rate constants to ones calculated for a standard set is smaller than unit for 2.7, 1.9, 1.4 μm bands at all heights. For 2.7 μm, the ratio becomes equal to ~0.7 below 60 km.

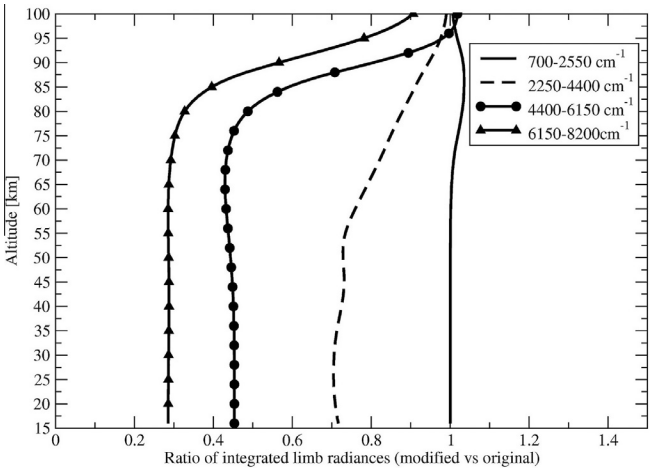

Fig. 4. Integrated limb radiances for 6.3 μm (700–2550 cm^{-1}), 2.7 μm (2250–4400 cm^{-1}), 1.9 μm (4400–6150 cm^{-1}), and 1.4 μm (6150–8200 cm^{-1}) bands.

For 1.9 and 1.4 μm bands, the ratios decrease to 0.45 and 0.3, respectively, at ~70 km height. The 6.3 μm band is the least affected one, with the ratio slightly more than a unit in the altitude range of 70–95 km reaching 1.03 at 85 km and equal to one at the other altitudes. A conclusion, which can be made from this figure is that the rate coefficient under consideration will not affect the estimates of the energetics of the MLT area and will not affect the H_2O VMR retrievals from the 6.3 μm channel of broadband radiometers like SABER/TIMED (Russell et al., 1999). It is obvious, though, that the retrievals in the other bands will be significantly affected. To study the effects of k change on the spectrally resolved radiance, we have built joint multi-panel plots, which demonstrate several aspects of calculated limb radiances.

Figs. 5 and 6 present the spectral characteristics of limb radiance at 90 and 50 km height, respectively, and consist of 16 panels each. The columns from left to right refer to 6.3, 2.7, 1.9, and 1.4 μm bands. An altitude of 50 km has been chosen as a lower limit since it is an approximate height of LTE breakdown for $H_2O(\nu_2)$-levels (Fig. 2) while the upper limit of 90 km is defined by H_2O abundance in Earth's atmosphere. We have to note here that the results in Figs. 5 and 6 will depend on the instrumental function halfwidth, and the narrower the function, the stronger the variation in differences and ratios, so for demonstration purposes the monochromatic line intensities for these plots have been convolved with 10 cm^{-1} triangular instrumental function. The upper row shows spectral limb radiances in the absolute units, calculated for an updated k. The second row from the top gives an insight on the contributions of different transitions to the spectrum. In the next row, the differences between spectral radiances calculated for an updated and standard sets of rate constants have been built in absolute units.

Finally, the bottom panel shows the ratio of radiances estimated at the wavelengths where the radiance is greater than 1% of the maximal value of the corresponding band. The latter filtering is necessary to get rid of non-informative weak lines, which will mask the effects in stronger lines by "zero divided by zero"-like patterns. It is obvious from the upper rows of Figs. 5 and 6 that the intensities of radiances in 2.7, 1.9 and 1.4 μm bands are stronger w.r.t. that of 6.3 μm band at 90 km than at 50 km. This is explained by differences in pumping mechanisms for the corresponding upper vibrational levels during daytime: the $H_2O(\nu_2)$ levels are pumped by radiance coming from below while the levels responsible for the formation of radiance in 2.7, 1.9, and 1.4 μm bands, namely, (001;100), (011 and 021), and 101, respectively, are pumped by solar radiance coming from the top of the atmosphere.

It is interesting to trace the behavior of the main contributors to the considered H_2O ro-vibrational bands at 50 and 90 km heights (compare the second rows of Figs. 5 and 6). For 6.3 μm band at 50 km, the contribution of the 020 → 010 transition is negligible in comparison with that of the fundamental band, while at 90 km two hot bands, 020 → 010 and 030 → 020 should be taken into account. For 2.7 μm band, the contributions of the 001 → 000 and 100 → 000 transitions are much stronger at 90 km than at 50 km because of the quenching effects differences: at higher altitudes, the collisions are less frequent, and the vibrational quantum has more time to be emitted rather than quenched. This can be seen in the (001;100) T_{vib} behavior in Fig. 2: at 50 km they are close to T_{kin} while at 90 km they are warmer than T_{kin} by 250 and 275 K, respectively. For 1.9 and 1.4 μm bands, the contributions almost do not change with height that is explained both by the corresponding T_{vib} values and by the limb observation geometry where the upper layers contribute to signal

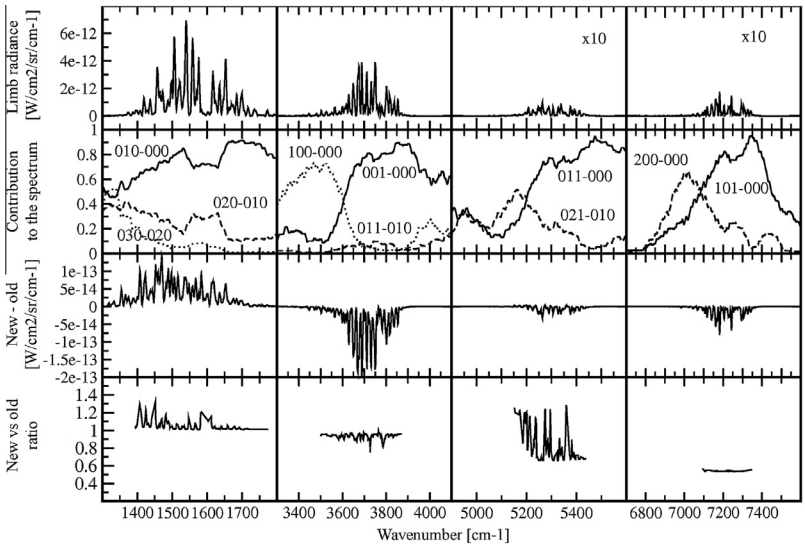

Fig. 5. Sensitivity of simulated limb spectra to k in 6.3, 2.7, 1.9, and 1.4 μm bands at 90 km. Upper row: limb radiance in absolute values for updated set of rate coefficients; second row: contribution of three most important transitions to a given band radiance; third row: difference between limb radiation calculated for an updated and standard sets of rates; bottom row: ratio of limb radiation calculated for an updated and standard set of rates.

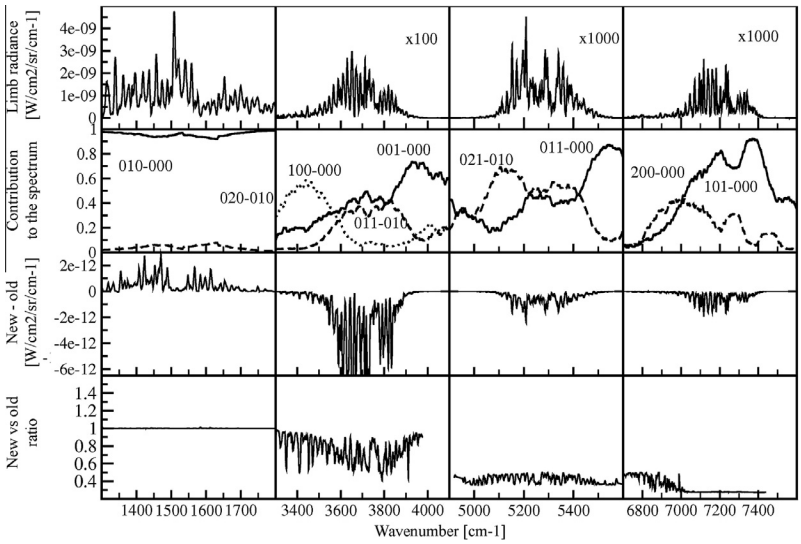

Fig. 6. Sensitivity of simulated limb spectra to k in 6.3, 2.7, 1.9, and 1.4 μm bands at 50 km. See the panel description of Fig. 5.

observed for lower tangent heights: the effect is created by a convolution of strongly solar-pumped levels in the upper atmospheric layers with the H_2O concentration, which decreases with height.

The third row in Figs. 5 and 6 provides an insight of solar energy redistribution within the system of H_2O vibrational levels. The mechanisms and qualitative effects are the same for all of the heights under consideration: stronger quenching of the solar-pumped levels leads to a decrease in their populations (Fig. 2) and to an increase of the population of lower energy levels. The net effect is that the radiance in 2.7, 1.9, and 1.4 μm bands becomes smaller while the 6.3 μm radiance increases. In absolute values, the effects are comparable in magnitude in all bands, but the relative importance of the change, shown in the bottom rows is different: the 1.9 and 1.4 μm bands experience strong changes with up to 70% decrease in intensity at 50 km height while the 2.7 μm band radiance shows larger absolute, but smaller relative changes than these two bands. The sensitivity of the 6.3 μm band radiance to k changes is almost negligible at 50 km and is up to 20% at 90 km height, that is explained by the behavior of the contributors' T_{vib} (see Fig. 2 and the second rows in Figs. 5 and 6).

5. Retrieval uncertainties: safe and unsafe microwindows

The last paragraph of Section 4 and the analysis of Fig. 4 and the bottom rows of Figs. 5 and 6 lead to the following statements important for the satellite remote sensing. The uncertainties and changes in k: (a) do not affect the H_2O retrievals from broadband 6.3 μm emissions detected by space-borne radiometers like SABER/TIMED; (b) do affect the retrievals from broadband measurements in 2.7, 1.9, and 1.4 μm bands; (c) may affect the retrievals from spectrally resolved signals in all considered bands if the spectral points for analysis (so-called "microwindows") are picked up without referring to sensitivity plots shown in bottom rows of Figs. 5 and 6. While the (a) and (b) statements are self-evident and do not require further comments, the third statement needs more explanations in regard to its applicability to signals from space-borne spectrometers like, e.g. MIPAS onboard the Envisat (Milz et al., 2005).

To address these issues, we introduced a concept of "safe" and "unsafe" microwindows. The idea is to identify microwindows used for the retrievals in such a way that the uncertainty of the retrieval caused by uncertainties in k is minimal. To do so, we have convolved the monochromatic limb radiance calculated for an updated and standard k with 2 cm^{-1} wide rectangular instrumental function for the microwindows centered 2 cm^{-1} apart of each other. The resulting spectra were analyzed for relative changes and the results are presented in Fig. 7. The color in Fig. 7 marks the "quality" of the microwindow, regardless of the sign of the change: if the radiance calculated for an updated k is 1.5 times larger or 1.5 times smaller than that calculated for a standard k, the line is marked with color corresponding to 50% change. As one can see, the whole 6.3 μm band is safe except for few points at 80 km height while the 2.7, 1.9, and 1.4 μm bands have a large number of unsafe microwindows, and some of them demonstrate changes exceeding 100% for the 1.4 μm band. The number of unsafe windows for the latter 3 bands decreases with height since the quenching becomes less efficient. For the 6.3 μm, the altitude of maximal effect is ~80 km, that is explained by an efficient quenching of the main contributing level, 010, below ~75 km height leading to LTE (Fig. 2) and rapid decrease of vibrational population of this level from the upper ones above 90 km height due to aforementioned decrease of quenching.

We have tested the microwindows used for the H_2O VMR retrievals in MIPAS experiment (see Table 1 of Milz et al. (2005) and Table A of von Clarmann et al. (2009)) and have found that their microwindows are safe

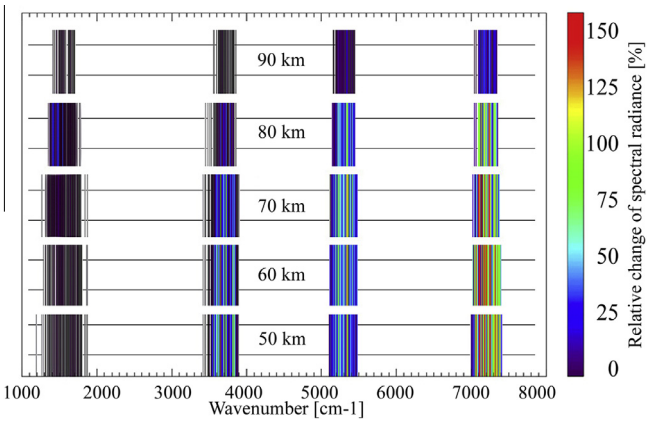

Fig. 7. Safe and unsafe microwindows for 50, 60, 70, 80 and 90 km: vertical lines mark the positions of strong spectral lines in the spectrum at different heights, line color denotes a relative change in spectral radiance (positive and negative changes of the same magnitude are marked by the same color, see the third rows of Figs. 5 and 6 for more details). (For interpretation of the references to color in this figure legend, the reader is referred to the web version of this article.)

at all heights. However, as follows from the Table 1 of (López-Puertas et al., 2005), the MIPAS spectral ranges (B) 1215–1500 cm^{-1} and (C) 1570–1750 cm^{-1} contain a number of unsafe microwindows, for which the change in calculated radiance is ~20–25% because of the hot transitions 020 → 010 and 030 → 020 contributing to the spectra. Most probably, this has a negligible effect on the H_2O VMR since MIPAS retrievals do not reach the altitudes marked as unsafe in Fig. 7, but this might become an issue for the future spectral instruments aimed at the MLT. The total list of safe and unsafe microwindows, composed from the worst column values in 50–90 km altitude region is available for download in the supplementary materials for the article.

6. Conclusions

We have studied the sensitivity of the H_2O vibrational level populations and the atmospheric spectral and integrated limb radiances for 6.3, 2.7, 1.9, and 1.4 μm bands in the MLT to the rate constant of intra-molecular V–V exchanges at which the second vibrational number ν_2 increases by two and the first or the third quantum number decreases by one. It has been found that current uncertainty of this rate coefficient affects several aspects of the non-LTE problem for H_2O in the MLT. Below we list the most important findings of this study.

1. The sensitivity of some vibrational levels to the rate constant under consideration (k) is quite high: the difference between T_{vib} calculated for updated and standard rate constants reaches 40–45 K for the upper vibrational levels (corresponds to 3–5 times change in level's population). Above 80–85 km, the T_{vib} calculated for updated k exceed that calculated for a standard k for levels with bending mode quantum number 2, 3 and 4. For 040, this excess reaches 45 K at 95 km (~5 times change in population). For the other levels and even for levels 021, 120 below 85 km, the T_{vib} calculated for updated k are smaller than the ones calculated for standard k. For 200, this difference reaches 40 K at 85 km (~3 times change in population). The behavior of T_{vib} differences is explained by kinetic mechanisms for the corresponding levels: stronger quenching of the upper 3 levels in our model leads to decrease of their populations, transferring more energy from these levels to lower-lying 040 and 030, which demonstrate an increase in population in the middle atmosphere. The 110 and 011 levels also act as donors to lower-lying levels while 021 and 120 work as donors below ~85 km height and as acceptors above this height.
2. The changes in k do not affect the estimates of the energetics of the MLT area. For the 6.3 μm band, the ratio of integrated limb intensities calculated for an updated k to ones calculated for a standard k is just slightly greater than a unit in the altitude range of 70–95 km reaching 1.03 at 85 km and equal to one at the other altitudes. However, for the 2.7, 1.9, 1.4 μm bands, the rate constants change leads to 30–70% decrease of the band limb radiances below 60–75 km.
3. The stronger quenching of the solar-pumped levels at new k leads to a decrease in their populations and to an increase of the population of lower energy levels. The net effect is that the spectral radiance in 2.7, 1.9, and 1.4 μm bands becomes smaller while the 6.3 μm radiance slightly increases. The ratio of spectral limb intensities calculated for updated and standard k depends on the band and on the height of LTE assumption breakdown. The strongest effect in simulated radiance was observed for 1.4 μm band at 50 km height.
4. The uncertainty in k value can contribute to H_2O retrieval uncertainties. As we estimated, this does not affect [H_2O] retrievals either from infrared radiation measured by limb scanning broadband infrared radiometer SABER or from MIPAS observations (Milz et al., 2005; von Clarmann et al., 2009). However, for the spectrally resolved H_2O bands, there are microwindows, which demonstrate significant changes in calculated intensity. Even for 6.3 μm band, some spectral radiances at 80 km change by more than 20–25% because of the hot transitions 020 → 010 and 030 → 020 contributing to the spectra. In 50–90 km altitude region, this change reaches 50% for 2.7 μm band, 75% for 1.9 μm band, and more than 100% for 1.4 μm band radiances. The total list of "safe" and "unsafe" microwindows, composed from the worst column values in 50–90 km altitude region is available for download in the supplementary materials for the article.

We conclude that an understanding of the nonequilibrium radiation in IR ro-vibrational H_2O bands cannot be complete without knowing the values of rate constants of main processes of H_2O vibrational relaxation (1–6). The

present study is based on the works of Zittel and Masturzo (1991) and Barnes et al. (2004) who showed that the rate coefficients of (6) and (7) strongly depend on the energy of the upper vibrational level. Therefore, using a single k for all reactions of type (6) and (7) is fundamentally wrong. We have shown that currently accepted practice of using the same k for all processes of type (6) and (7) can lead to errors both in calculating the vibrational level populations and in H_2O concentration retrievals from the IR spectral radiance in the MLT.

Appendix A. Supplementary data

Supplementary data associated with this article can be found, in the online version, at http://dx.doi.org/10.1016/j.asr.2014.12.002.

References

Barnes, P.W., Sims, I.R., Smith, I.W.M., 2004. Relaxation of H_2O from its 04 vibrational state in collisions with H_2O, Ar, H_2, N_2, and O_2. J. Chem. Phys. 120 (12), 5592–5600.

Bernath, P.F., McElroy, C.T., Abrams, M.C., Boone, C.D., Butler, M., Camy-Peyret, C., Carleer, M., Clerbaux, C., Coheur, P.F., Colin, R., DeCola, P., DeMazi‘ ere, M., Drummond, J.R., Dufour, D., Evans, W.F.J., Fast, H., Fussen, D., Gilbert, K., Jennings, D.E., Llewellyn, E.J., Lowe, R.P., Mahieu, E., McConnell, J.C., McHugh, M., McLeod, S.D., Michaud, R., Midwinter, C., Nassar, R., Nichitiu, F., Nowlan, C., Rinsland, C.P., Rochon, Y.J., Rowlands, N., Semeniuk, K., Simon, P., Skelton, R., Sloan, J.J., Soucy, M.-A., Strong, K., Tremblay, P., Turnbull, D., Walker, K.A., Walkty, I., Wardle, D.A., Wehrle, V., Zander, R., Zou, J., 2005. Atmospheric chemistry experiment (ACE): mission overview. Geophys. Res. Lett. 32, L15S01. http://dx.doi.org/10.1029/2005GL022386.

Gusev O.A., Kutepov A.A., 2003. Non-LTE gas in planetary atmospheres. In: Hubeny I, Mihalas D, Werner K (Eds.), Stellar Atmosphere Modeling, ASP Conference Series, vol. 288, pp. 318–330.

Feofilov, A.G., Kutepov, A.A., Pesnell, W.D., Goldberg, R.A., Marshall, B.T., Gordley, L.L., García-Comas, M., López-Puertas, M., Manuilova, R.O., Yankovsky, V.A., Petelina, S.V., Russell III, J.M., 2009. Daytime SABER/TIMED observations of water vapor in the mesosphere: retrieval approach and first results. Atmos. Chem. Phys. 9, 8139–8158.

Feofilov, A.G., Kutepov, A.A., She, C.-Y., Smith, A.K., Pesnell, W.D., Goldberg, R.A., 2012. $CO_2(\nu_2)$-O quenching rate coefficient derived from coincidental SABER/TIMED and Fort Collins lidar observations of the mesosphere and lower thermosphere. Atmos. Chem. Phys. 12, 9013–9023.

Feofilov, A.G., Kutepov, A.A., 2012. Infrared radiation in the mesosphere and lower thermosphere: energetic effects and remote sensing. Surv. Geophys. 33 (6), 1231–1280. http://dx.doi.org/10.1007/s10712-012-9204-0.

Finzi, J., Hovis, F.E., Panfilov, V.N., Hess, P., Moore, C.B., 1977. Vibrational relaxation of water vapor. J. Chem. Phys. 67 (9), 4053–4061.

Funke, B., López-Puertas, M., Garcia-Comas, M., Kaufmann, M., Hopfner, M., Stiller, G.P., 2012. GRANADA: a generic RAdiative traNsfer AnD non-LTE population algorithm. J. Quant. Spectrosc. Radiat. Transfer 113 (14), 1771–1817.

Kutepov, A.A., Gusev, O.A., Ogibalov, V.P., 1998. Solution of the non-LTE problem for molecular gas in planetary atmospheres: superiority of accelerated lambda iteration. J. Quant. Spectrosc. Radiat. Transfer 60 (2), 199–220.

López-Puertas, M., Zaragoza, G., Kerridge, B.J., Taylor, F.W., 1995. Non-local thermodynamic equilibrium model for H_2O 6.3 and 2.7 μm bands in the middle atmosphere. J. Geophys. Res. 100 (D5), 9131–9147. http://dx.doi.org/10.1029/95JD00383.

López-Puertas, M., Funke, B., Gil-López, S., López-Valverde, M.Á., von Clarmann, T., Fischer, H., Oelhaf, H., Stiller, G., Kaufmann, M., Koukouli, M.E., Flaud, J.-M., 2005. Atmospheric non-local thermodynamic equilibrium emissions as observed by the Michelson interferometer for passive atmospheric sounding (MIPAS). Spectrosc. Planet. Atmos. 6, 848–863, http://france.elsevier.com/direct/COMREN/.

Manuilova, R.O., Shved, G.M., 1985. The 2.7 and 6.3 m H_2O emissions in the middle atmosphere. J. Atmos. Terr. Phys. 47 (5), 413–422.

Manuilova, R.O., Yankovsky, V.A., Gusev, O.A., Kutepov, A.A., Sulakshina, O.N., Borkov, Yu.G., 2001. Non-equilibrium emission of the middle atmosphere in the IR rovibrational water vapor bands. Atmos. Ocean. Opt. 14 (10), 864–867.

Milz, M., von Clarmann, T., Fischer, H., Glatthor, N., Grabowski, U., Hopfner, M., Kellmann, S., Kiefer, M., Linden, A., Mengistu, Tsidu G., Steck, T., Stiller, G.P., Funke, B., Lopez-Puertas, M., Koukouli, M.E., 2005. Water vapor distributions measured with the Michelson interferometer for passive atmospheric sounding on board Envisat (MIPAS/Envisat). J. Geophys. Res. 110, D24307. http://dx.doi.org/10.1029/2005JD005973.

Rothman, L.S., Gordon, I.E., Barbe, A., Chris Benner, D., Bernath, P.F., Birk, M., Boudon, V., Brown, L.R., Campargue, A., Champion, J.-P., Chance, K., Coudert, L.H., Dana, V., Devi, V.M., Fally, S., Flaud, J.-M., Gamache, R.R., Goldman, A., Jacquemart, D., Kleiner, I., Lacome, N., Lafferty, W.J., Mandin, J.-Y., Massie, S.T., Mikhailenko, S.N., Miller, C.E., Moazzen-Ahmadi, N., Naumenko, O.V., Nikitin, A.V., Orphal, J., Perevalov, V.I., Perrin, A., Predoi-Cross, A., Rinsland, C.P., Rotger, M., Simecková, M., Smith, M.A.H., Sung, K., Tashkun, S.A., Tennyson, J., Toth, R.A., Vandaele, A.C., Vander Auwera, J., 2009. The HITRAN 2008 molecular spectroscopic database. J. Quant. Spectrosc. Rad. Transfer 110 (9–10), 533–572.

Russell III, J.M., Mlynczak, M.G., Gordley, L.L., Tansock, J.J., Esplin, R.W., 1999. An overview of the SABER experiment and preliminary calibration results. SPIE 3756, 277–288.

von Clarmann, T., Hopfner, M., Kellmann, S., Linden, A., Chauhan, S., Funke, B., Grabowski, U., Glatthor, N., Kiefer, M., Schieferdecker, T., Stiller, G.P., Versick, S., 2009. Retrieval of temperature, H_2O, O_3, HNO_3, CH_4, N_2O, $ClONO_2$ and ClO from MIPAS reduced resolution nominal mode limb emission measurements. Atmos. Meas. Tech. 2, 159–175, www.atmos-meas-tech.net/2/159/2009/.

Yankovsky, V.A., Babaev, A.S., 2011. Photolysis of O_3 at Hartley, Chappuis, Huggins, and Wulf Bands in the middle atmosphere: vibrational kinetics of oxygen molecules O_2(X3, v<=35). Atmos. Ocean. Opt. 24 (1), 6–16.

Zittel, P.F., Masturzo, P.F., 1991. Vibrational relaxation of H_2O by H_2, HCl, and H_2O at 295 K. J. Chem. Phys. 95 (11), 8005–8012.